Supplementary Information

Tuning Fe^{II}/Fe^{III} ratio by substituent regulation to improve peroxidase-like activity of metal–organic frameworks for sensitive biosensing

Keyu Xing[a], Siyao Peng[a], Mengting Liu[a], Lingli Long[a], Shaoyi Yu[a], Li Yao[a,d], Jian Zhang[c], Maolong Chen[a], Yunhui Cheng[a] and Zhou Xu[a,b*]

[a] School of Food Science and Bioengineering, Changsha University of Science & Technology, Changsha 410114, China.

[b] State Key Laboratory of Utilization of Woody Oil Resource, Hunan Academy of Forestry, Changsha, 410004, Hunan, China

[c] College of Automotive and Mechanical Engineering, Changsha University of Science & Technology, Changsha 410114, China.

[d] College of Food and Biological Engineering, Hefei University of Technology, Hefei 230009, China.

*Corresponding email address: xz_jnu@126.com

Table of Contents

Supplementary Information

1. Supporting Methods

1.1 Chemicals and reagents

$FeCl_3 \cdot 6H_2O$ (97%), 2-aminoterephthalic acid, terephthalic acid, 2-nitroterephthalic acid, 2-bromoterephthalic acid, 2,5-dihydroxyterephthalic acid, CH_3COOH (99.7%), acetone, natrium aceticum (CH_3COONa), p-benzoquinone, dimethylformamide (DMF), 5,5-dimethyl-1-pyrroline-1-oxide (DMPO), methanol, and glucose oxidase (GOx) were all purchased from Sigma-Aldrich. 3,3′,5,5′-tetramethylbenzidine (TMB), H_2O_2, glucose, fructose, maltose, and lactose were all purchased from Sinopharm Chemical Reagent Company. Millipore Milli-Q ultrapure (18.2 MΩ; Merck-Millipore, Darmstadt, Germany) water was used throughout the whole study. All other reagents were of analytical reagent grade.

1.2 Instrumentation

Fluorescence absorption spectrum measurement was carried out in an F-7000 fluorophotometer. Ultraviolet-visible (UV-vis) absorption spectrum measurements were carried out in a UV-2550 spectrophotometer. A Tecnai G2 F20 transmission electron microscope (TEM) with an accelerating voltage of 200 kV was used for imaging to observe the morphology of MOFs. The BRUKER AXS D8-Advance X-ray diffraction (XRD) system was used to study the crystalline phase. X-ray photoelectron spectroscopy (XPS) measurements were performed on a Thermo Scientific ESCALAB 250 spectrometer. Electron spin resonance (ESR) signal was obtained on a Bruker ESP 300E (X-band) spectrometer.

1.3 Synthesis and characterization of MOFs

MIL-88-H

Synthesis (the material here is called MIL-88-H-as; “as” stands for “as-synthesized”): $FeCl_3 \cdot 6H_2O$ (1 mmol, 270 mg) and terephthalic acid (1 mmol, 166 mg) were dissolved into DMF (5 mL) and 2 M NaOH (0.4 mL). The mixture was transferred to a Teflon lined autoclave and heated for 12 h at 373 K. After cooling to room temperature, the mixture was centrifuged and washed with acetone and water, respectively.

Activation: The powder was dispersed into 20 mL of MeOH and stirred for 16 h. The material was centrifuged and washed with MeOH until the supernatant became colorless. Finally, the MOF was dried at 353 K under air before being collected.

MIL-88-NH_2

Synthesis: $FeCl_3 \cdot 6H_2O$ (1 mmol; 270 mg) and 2-aminoterephthalic acid (1 mmol, 181 mg) were dissolved into MeOH (15 mL). The mixture was transferred to a Teflon lined autoclave and heated for 24 h at 373 K. After cooling to room temperature, the mixture was centrifuged and washed with acetone and water, respectively.

Activation: The powder was dispersed into 20 mL of MeOH and stirred for 16 h. The material was centrifuged and washed with MeOH until the supernatant became colorless. Finally, the MOF was dried at 353 K under air before being collected.

MIL-88-$(OH)_2$

Synthesis: Fe $(ClO_4)_3 \cdot nH_2O$ (1 mmol, 354 mg) and 2, 5-dihydroxyterephthalic acid (1 mmol, 198 mg) were dissolved into DMF (5 mL). The mixture was transferred to a Teflon lined autoclave and heated for 12 h at 353 K. After cooling to room temperature, the mixture was centrifuged and washed with acetone and water, respectively.

Activation: The powder was dispersed into 20 mL of MeOH and stirred for 16 h. The material was centrifuged and washed with MeOH until the supernatant became colorless. Finally, the MOF was dried at 353 K under air before being collected.

MIL-88-NO_2

Synthesis: $FeCl_3 \cdot 6H_2O$ (1 mmol, 270 mg) and nitroterephthalic acid (1 mmol, 211 mg) were dissolved into distilled water (5 mL). The mixture was transferred to a Teflon lined autoclave and heated for 12 h at 373 K. After cooling to room temperature, the mixture was centrifuged and washed with acetone and water, respectively.

Activation: The powder was dispersed into 10 mL of EtOH and stirred for 16 h. The material was centrifuged and washed with EtOH until the supernatant became colorless. Finally, the MOF was dried at 353 K under air before being collected.

MIL-88-Br

Synthesis: $FeCl_3·6H_2O$ (1 mmol, 270 mg) and 2-bromoterephthalic acid (1 mmol, 245 mg) were dissolved into DMF (5 mL). The mixture was transferred to a Teflon lined autoclave and heated for 12 h at 373 K. After cooling to room temperature, the mixture was centrifuged and washed with acetone and water, respectively.

Activation: The powder was dispersed into 20 mL of DMF and stirred for 16 h. The material was centrifuged and washed with DMF until the supernatant became colorless. Finally, the MOF was dried at 353 K under air before being collected.

1.4 Kinetic analysis

The kinetic measurement was operated by recording the absorbance intensity at 450 nm on a UV–vis spectrophotometer. The experiment was implemented under the optimal conditions with a fixed concentration of TMB or H_2O_2. The kinetic parameters were calculated by the following equation.

$$\frac{1}{V0}=\frac{Km}{Vmax[S]}+\frac{1}{Vmax}$$

Where V represents the initial velocity; V_{max} is the maximum rate of reaction; K_m is the constant of Michaelis-Menten, and [S] presents the concentration of substrate (H_2O_2 or TMB).

1.5 Computational details

The first-principles calculations in this paper are all based on density functional theory (DFT). This method is implemented in the DMol software package of the material studio. The adsorption energy (E_{ads}) was calculated by the following equation, where the total energies of the surface with adsorbed molecules, the isolated surface and the isolated molecule were denoted by $E_{mol@surf}$, E_{surf}, and E_{mol} represent respectively.

$$E_{ads} = E_{mol@surf} - E_{surf} - E_{mol}$$

Supplementary Information

This paper uses high-precision convergence conditions to optimize the structure of the adsorption system. The PW91 exchange correlation functional is used to describe the exchange correlation energy with a generalized gradient approximation (GGA), and the kinetic energy cut-off value of all plane waves is set to 400eV. All-electron Kohn–Sham wave functions were expanded based on double numerical plus d-functions (DND). The convergence standards of relaxation for energy, gradient and atomic displacement are $2.0*10^{-5}$ Ha, 0.004 Ha/A° and 0.009 A°, respectively.

$$H_2O_2\ (aq) \rightarrow OH^* + \cdot OH \qquad \text{(equation S1)}$$

$$OH^* + \cdot OH \rightarrow O^* + H_2O^* \qquad \text{(equation S2)}$$

$$O^* + H_2O^* + (H^+ + e^-) \rightarrow OH^* + H_2O\ (aq) \qquad \text{(equation S3)}$$

$$OH^* + H_2O\ (aq) + (H^+ + e^-) \rightarrow 2H_2O\ (aq) \qquad \text{(equation S4)}$$

2. Supporting Figures

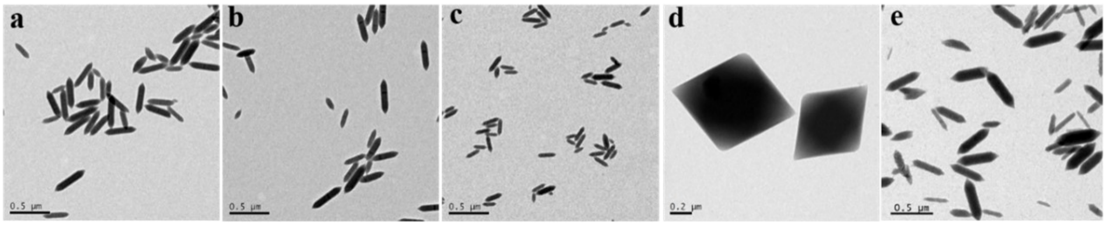

Fig. S1. The TEM images of MIL-88-NH_2 (a), MIL-88-NO_2 (b), MIL-88-H (c), MIL-88-$(OH)_2$ (d), and MIL-88-Br (e).

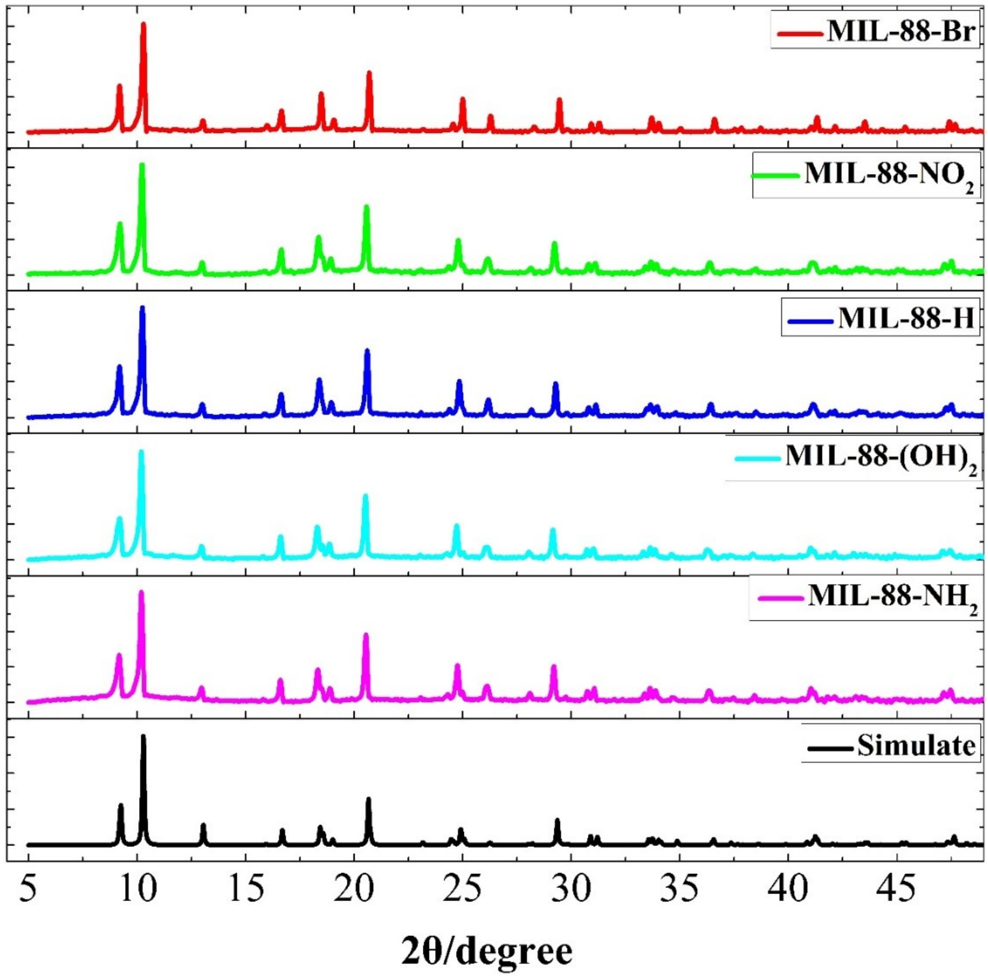

Fig. S2. The XRD images of MIL-88-R (R = NH_2, OH, H, NO_2, and Br).

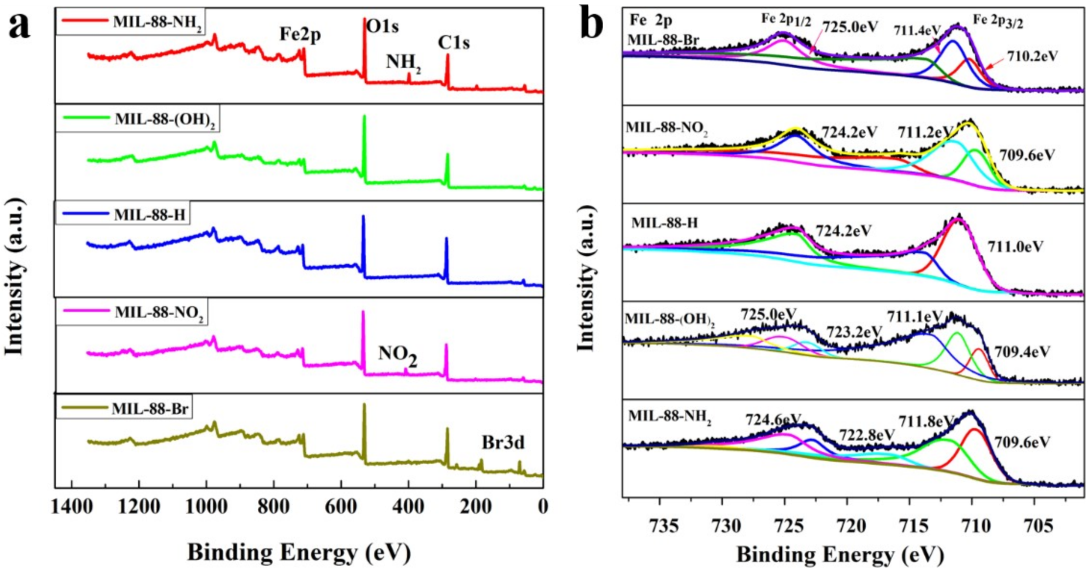

Fig. S3. The XPS spectra of MIL-88-R. (a) Full spectrum and (b) high-resolution scanning for Fe 2p region.

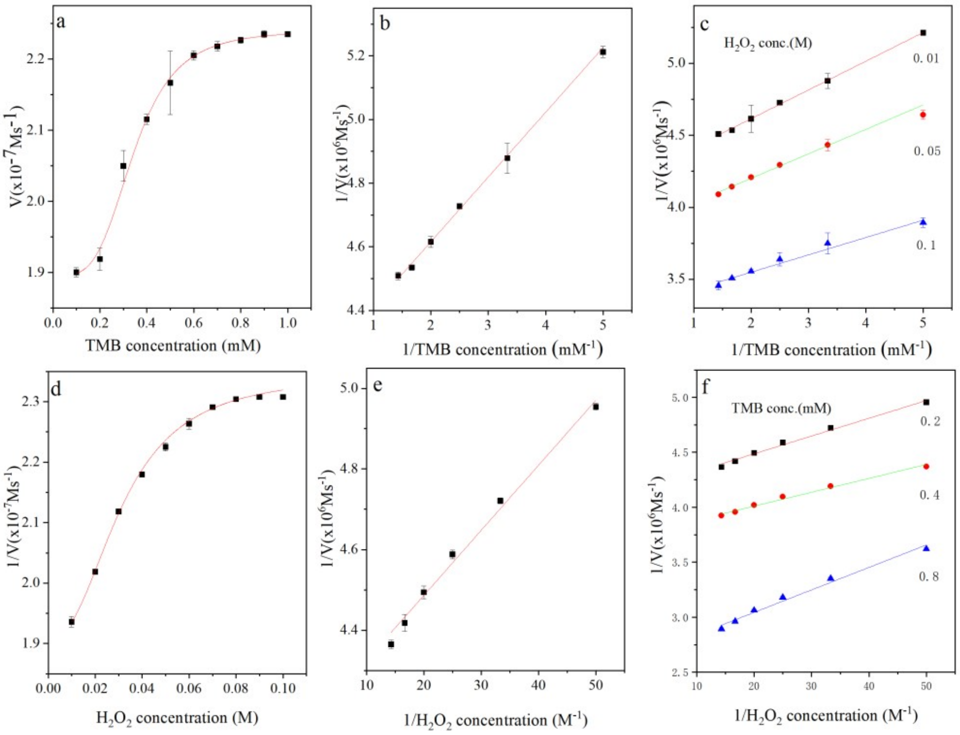

Fig. S4. The steady-state kinetics analysis of MIL-88-NH_2 by varying concentration of TMB (a) and H_2O_2 (d) and corresponding Lineweaver − Burk curve (b, c, e, and f).

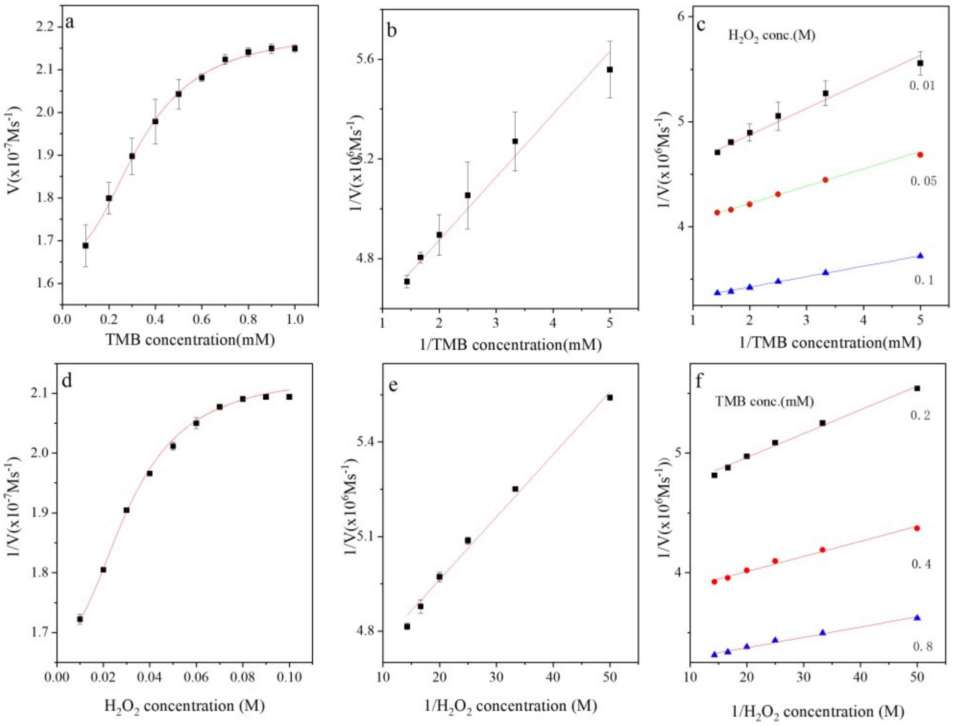

Fig. S5. The steady-state kinetics analysis of MIL-88-OH by varying concentration of TMB (a) and H_2O_2 (d) and corresponding Lineweaver − Burk curve (b, c, e, and f).

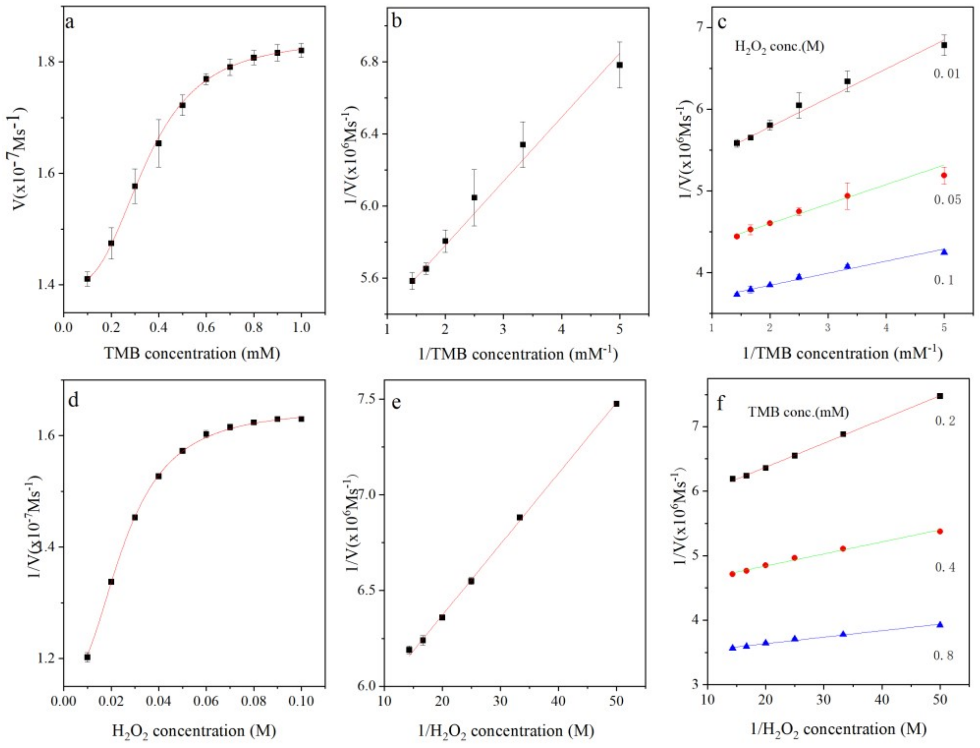

Fig. S6. The steady-state kinetics analysis of MIL-88 by varying concentration of TMB (a) and H_2O_2 (d) and corresponding Lineweaver − Burk curve (b, c, e, and f).

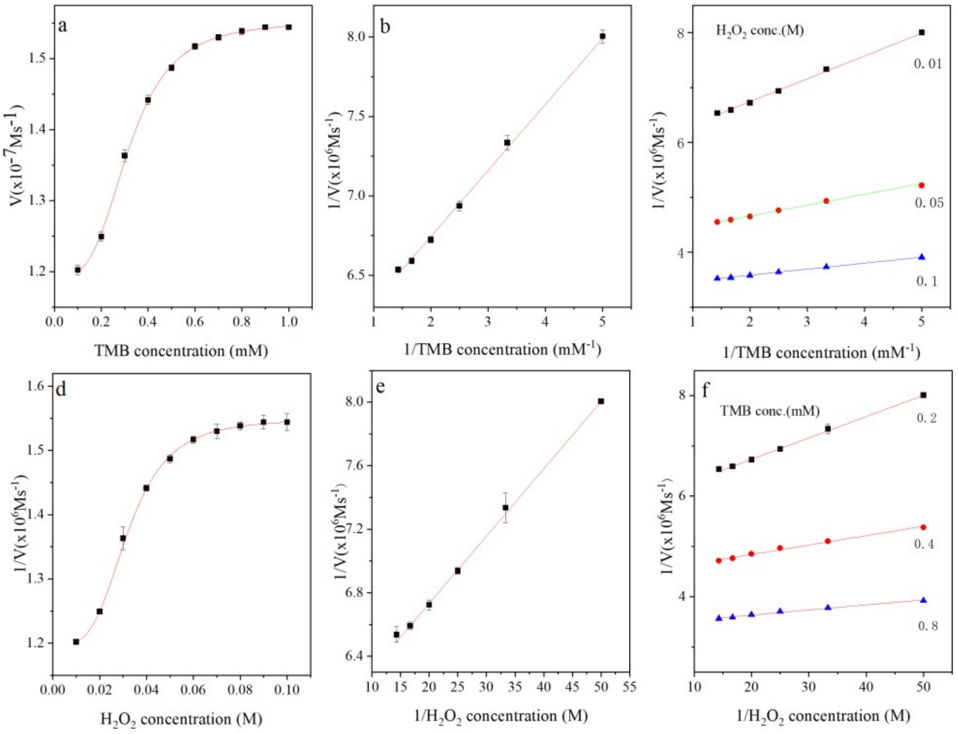

Fig. S7. The steady-state kinetics analysis of MIL-88-NO_2 by varying concentration of TMB (a) and H_2O_2 (d) and corresponding Lineweaver − Burk curve (b, c, e, and f).

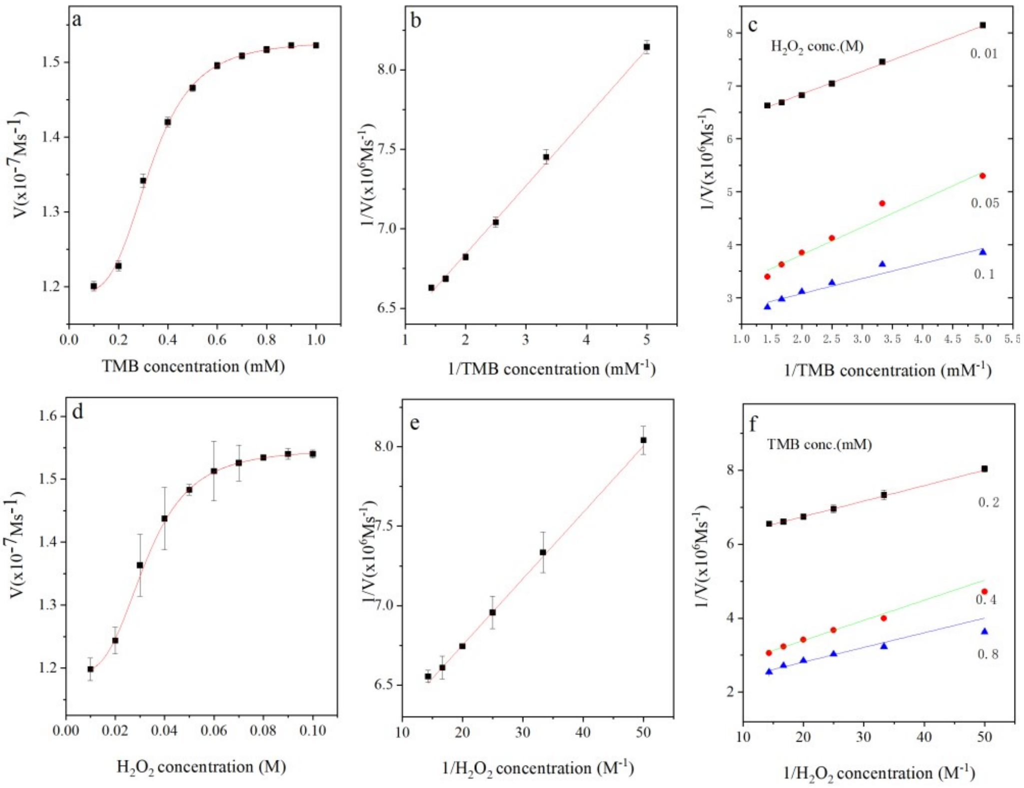

Fig. S8. The steady-state kinetics analysis of MIL-88-Br by varying concentration of TMB (a) and H_2O_2 (d) and corresponding Lineweaver − Burk curve (b, c, e, and f).

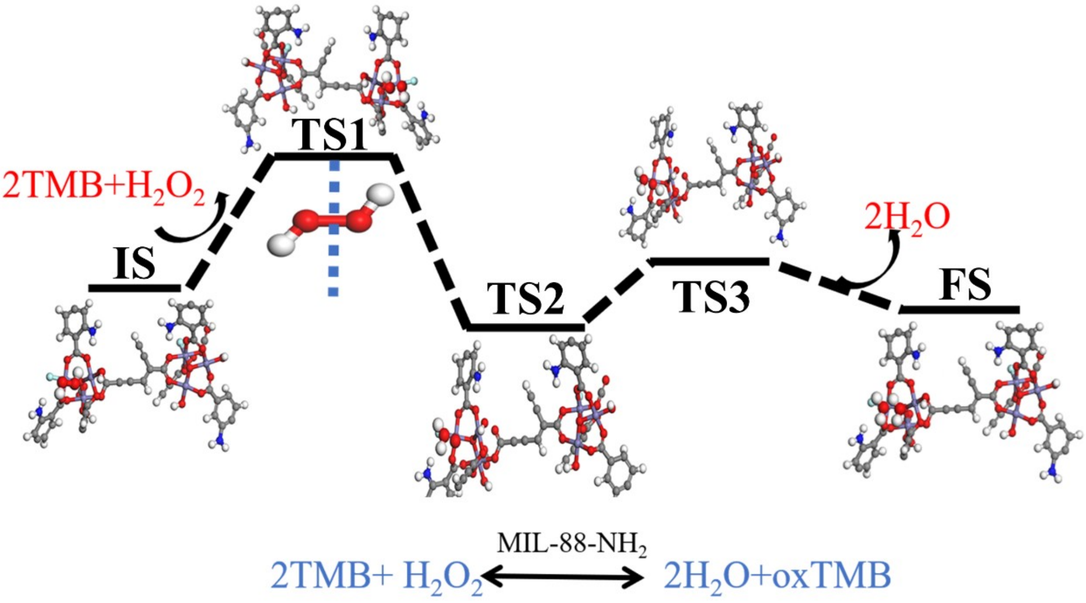

$MIL\text{-}88\text{-}NH_2 + H_2O_2 \leftrightarrow MIL\text{-}88\text{-}NH_2 + 2OH^*$ (equation S5)

$MIL\text{-}88\text{-}NH_2 + 2OH \leftrightarrow MIL\text{-}88\text{-}NH_2\text{-}\ O^* + H_2O^*$ (equation S6)

$MIL\text{-}88\text{-}NH_2\text{-}\ O^* + 2TMB + H_2O^* \leftrightarrow MIL\text{-}88\text{-}NH_2 + 2H_2O + oxTMB$ (equation S7)

Fig. S9. Potential energy profiles for H_2O_2 oxidation catalyzed by MIL-88-NH_2. The isolated clusters and reactant molecules in the gas phase are taken as zero-point potential energy.

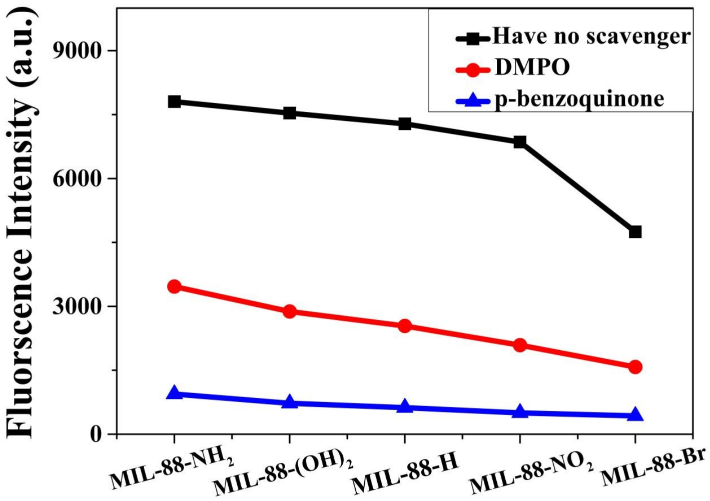

Fig. S10. The experiment of spin trapping of free radical intermediate. Fluorescence intensity without free radical capturing reagent (black), with free radical capturing reagent (red), and with free radical scavenger (blue).

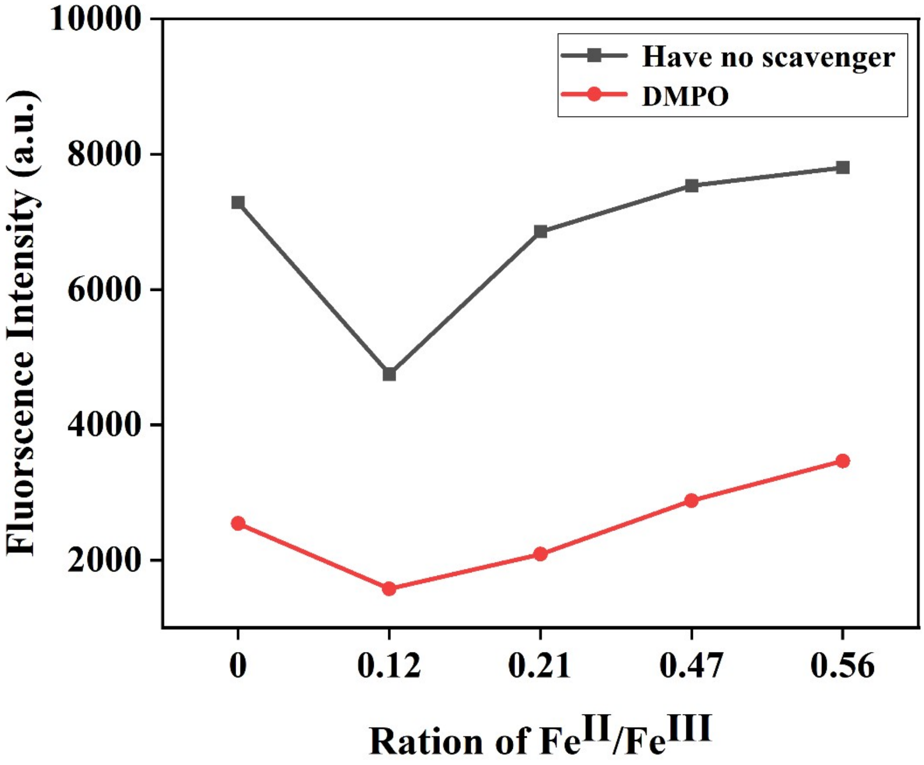

Fig. S11. The experiment of spin trapping of free radical intermediate in different ration of Fe^{II}/Fe^{III} without free radical capturing reagent (black), with free radical capturing reagent (red).

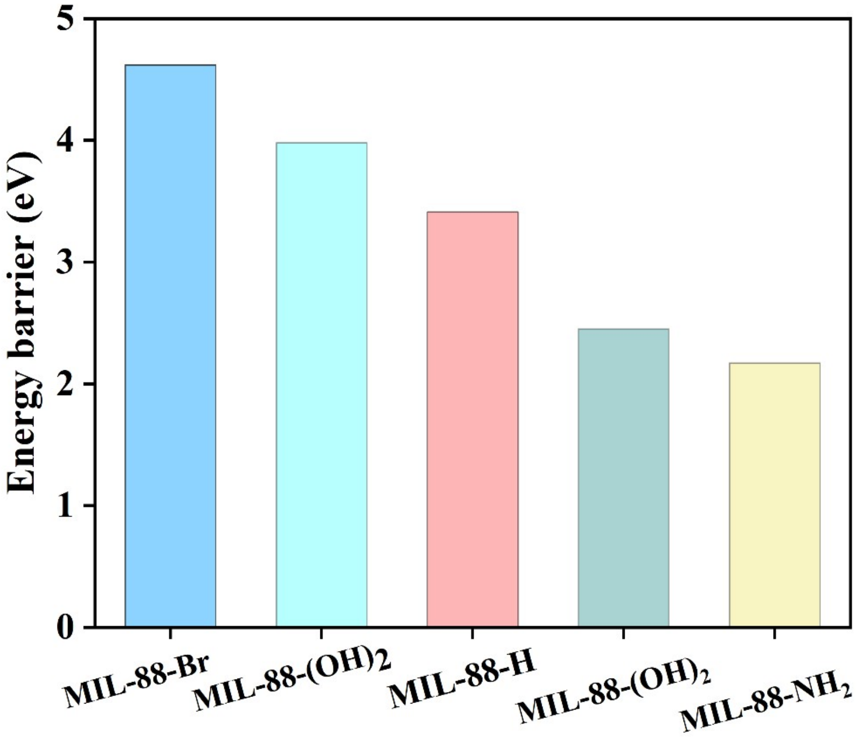

Fig. S12. The relationship between energy barrier and substituents in MIL-88-R.

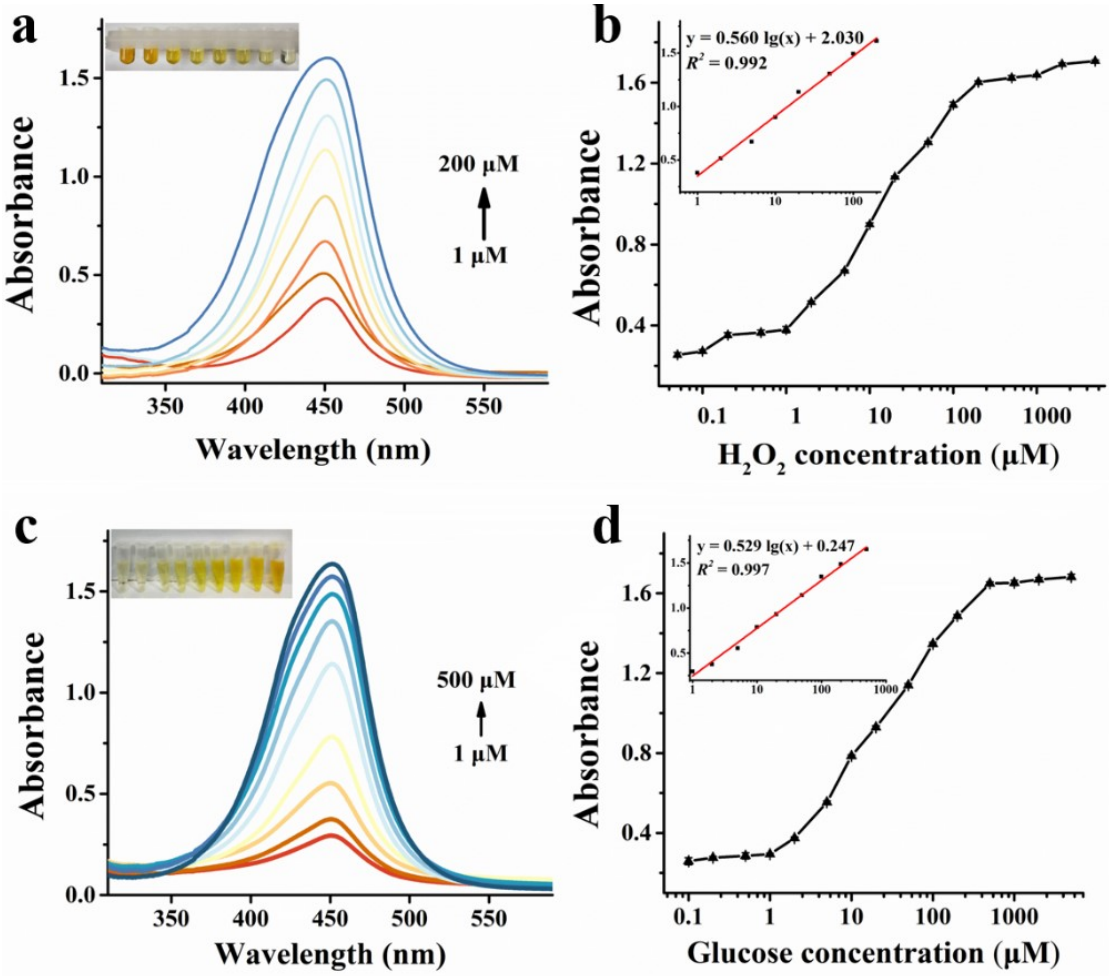

Fig. S13. Absorption spectra (a) and intensity (b) of MIL-88-NH_2 on oxTMB produced by H_2O_2 at different concentrations. Inset (a) showed the immunoassay photos in the presence of H_2O_2 at concentrations of 1, 2, 5, 10, 20, 50, 100, and 200 μM. Absorption spectrum (c) and intensity (d) of oxTMB produced by MIL-88-NH_2 with different concentrations of glucose. Inset (c) showed the immunoassay photos in the presence of glucose at concentrations of 1, 2, 5, 10, 20, 50, 100, 200 and 500 μM.

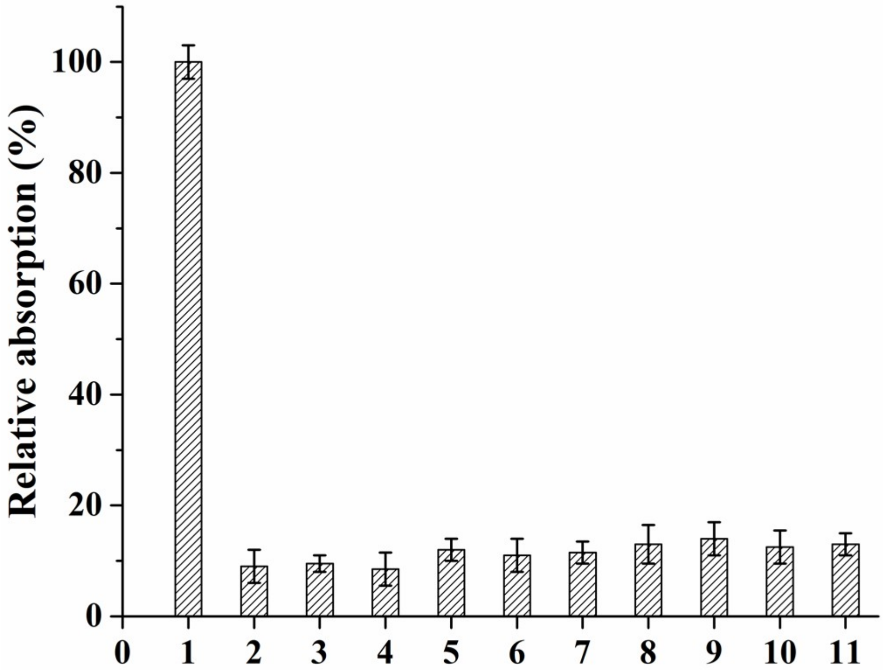

Fig. S14. Selectivity for detection of glucose by monitoring relative activities. The concentration of glucose was 0.1 mM. The concentrations of KCl, NaCl, uric acid, ascorbic acid, sodium citrate, urea, sucrose, fructose, and dopamine were 0.4 mM. The error bars represent the standard deviation of three measurements.

3. Supporting Tables

Table S1. Comparison of the kinetic parameters of various catalysts for the oxidation of TMB by H_2O_2

Catalysts	Substrates	K_m (10^{-3} M)	V_{max} (10^{-7} M s^{-1})	Ref.
HRP	TMB	0.43	1.00	1
	H_2O_2	3.70	0.87	1
MoS_2	TMB	4.37	0.24	2
	H_2O_2	4.78	0.20	2
MQDs	TMB	8.50	0.01	3
	H_2O_2	0.38	0.04	3
ZnN_4-SAEs	TMB	0.22	1.07	4
	H_2O_2	40.16	1.22	4
MoSA-N_3-C	TMB	0.79	1.12	5
	H_2O_2	2.00	3.70	5
c-$RuTe_2$	TMB	0.50	0.55	6
	H_2O_2	24.8	1.76	6
Fe-MIL-88-NH_2	TMB	4.83	2.38	This work
	H_2O_2	3.88	2.40	This work
Fe-MIL-88-$(OH)_2$	TMB	5.77	2.29	This work
	H_2O_2	4.35	2.19	This work
Fe-MIL-88	TMB	6.99	1.97	This work
	H_2O_2	6.58	1.77	This work

Catalysts	Substrates	K_m (10^{-3} M)	V_{max} (10^{-7} M s^{-1})	Ref.
Fe-MIL-88-NO_2	TMB	7.04	1.69	This work
	H_2O_2	7.20	1.70	This work
Fe-MIL-88-Br	TMB	7.17	1.67	This work
	H_2O_2	7.23	1.69	This work

Table S2. Selected bond distances for MIL-88-R (https://www.ccdc.cam.ac.uk/)

MIL-88-NH$_2$	MIL-88-(OH)$_2$	MIL-88-H	MIL-88-NO$_2$	MIL-88-Br
Fe1-O1 1.857	Fe1-O1 1.914	Fe1-O1 1.876	Fe1-O1 1.873	Fe1-O1 1.826
Fe1-O2 1.912	Fe1-O2 1.899	Fe1-O2 1.864	Fe1-O2 1.863	Fe1-O2 1.871
Fe1-O3 1.866	Fe1-O3 1.804	Fe1-O3 1.862	Fe1-O3 1.898	Fe1-O3 1.837
Fe1-O4 1.878	Fe1-O4 1.910	Fe1-O4 1.865	Fe1-O4 1.858	Fe1-O4 1.827
Fe1-O5 1.872	Fe1-O5 1.872	Fe1-O5 1.872	Fe1-O5 1.862	Fe1-O5 1.885
Fe1-O6 1.920	Fe1-O6 1.910	Fe1-O6 1.870	Fe1-O6 1.875	Fe1-O6 1.885
Fe2-O1 1.894	Fe2-O1 1.895	Fe2-O1 1.876	Fe2-O1 1.877	Fe2-O1 1.809
Fe2-O2 1.861	Fe2-O2 1.807	Fe2-O2 1.864	Fe2-O2 1.864	Fe2-O2 1.819
Fe2-O3 1.901	Fe2-O3 1.905	Fe2-O3 1.862	Fe2-O3 1.863	Fe2-O3 1.832
Fe2-O4 1.865	Fe2-O4 1.921	Fe2-O4 1.865	Fe2-O4 1.845	Fe2-O4 1.876
Fe3-Cl1 1.854	Fe3-Cl1 1.864	Fe3-Cl1 1.854	Fe3-Cl1 1.842	Fe3-Cl1 1.846
Fe3-O2 1.844	Fe3-O2 1.798	Fe3-O2 1.835	Fe3-O2 1.863	Fe3-O2 1.858
Fe3-O3 1.865	Fe3-O3 1.853	Fe3-O3 1.820	Fe3-O3 1.855	Fe3-O3 1.821
Fe3-O4 1.853	Fe3-O4 1.915	Fe3-O4 1.813	Fe3-O4 1.843	Fe3-O4 1.846
Fe4-O1 1.896	Fe4-O1 1.904	Fe4-O1 1.845	Fe4-O1 1.842	Fe4-O1 1.819
Fe4-O2 1.872	Fe4-O2 1.903	Fe4-O2 1.865	Fe4-O2 1.864	Fe4-O2 1.874
Fe4-O3 1.888	Fe4-O3 1.794	Fe4-O3 1.828	Fe4-O3 1.888	Fe4-O3 1.832
Fe4-O4 1.856	Fe4-O4 1.846	Fe4-O4 1.856	Fe4-O4 1.856	Fe4-O4 1.822
Fe5-Cl1 1.847	Fe5-Cl1 1.864	Fe5-Cl1 1.876	Fe5-Cl1 1.842	Fe5-Cl1 1.847
Fe5-O2 1.836	Fe5-O2 1.800	Fe5-O2 1.865	Fe5-O2 1.836	Fe5-O2 1.824
Fe5-O3 1.856	Fe5-O3 1.864	Fe5-O3 1.816	Fe5-O3 1.888	Fe5-O3 1.845
Fe5-O4 1.833	Fe5-O4 1.792	Fe5-O4 1.833	Fe5-O4 1.888	Fe5-O4 1.845
Fe5-O5 1.860	Fe5-O5 1.931	Fe5-O5 1.820	Fe5-O5 1.860	Fe5-O5 1.845
Fe5-O6 1.915	Fe5-O6 1.905	Fe5-O6 1.895	Fe5-O6 1.867	Fe5-O6 1.889
Fe6-O1 1.895	Fe6-O1 1.897	Fe6-O1 1.876	Fe6-O1 1.875	Fe6-O1 1.832
Fe6-O2 1.846	Fe6-O2 1.795	Fe6-O2 1.864	Fe6-O2 1.864	Fe6-O2 1.847
Fe6-O3 1.866	Fe6-O3 1.876	Fe6-O3 1.826	Fe6-O3 1.846	Fe6-O3 1.830
Fe6-O4 1.875	Fe6-O4 1.865	Fe6-O4 1.793	Fe6-O4 1.835	Fe6-O4 1.853

Table S3. H_2O_2 and TMB chemisorption structures, chemisorption energies ($E_{ads, H2O2}$ and $E_{ads, TMB}$) and calculated average bonding energies

Absorbate	$E_{ads, H2O2}$ (eV)	$E_{ads, TMB}$ (eV)	E_b (eV)
MIL-88-Br	1.37	1.61	-2.69
MIL-88-NO_2	-1.60	-1.73	-2.36
MIL-88-H	-1.80	-1.87	-0.84
MIL-88-$(OH)_2$	-1.92	-2.15	-0.71
MIL-88-NH_2	-2.32	-3.14	-0.65

Table S4. Comparison of glucose concentrations in serum samples determined using the constructed biosensor and reference values provided by a hospital.

Samples	Detected glucose concentration by conventional enzymatic method[a] (mM)	Detected glucose concentration by the developed biosensor (mM)[b] (mean ± SD[c])	CV [d] (%)
1	5.25	5.40 ± 0.2	3.7
2	5.49	5.64 ± 0.3	5.3
3	5.49	5.58 ± 0.3	5.4

a: Detected using a commercial glucose assay kit at the Hospital of Chinese Traditional and Western Medicine.

b: Detected using the constructed biosensor.

c: SD, Standard deviation; n =3.

d: CV, Coefficient of Variation = (SD/mean) × 100 %.

4. Supporting References

1. L .Z. Gao, J. Zhuang, L. Nie, J. B. Zhang, Y. Zhang, N. Gu, T. H. Wang, J. Feng, D. L. Yang, S. Perrett and X. Y. Yan, *Nat. Nanotechnol*. 2007, **2**, 577–583.

2. F. Feng, Y. H. Zhang, X. Zhang, B. Mu, J. H. Zhang, W. J. Qu, W. S. Tong, M. M. Liang, Q. An, Z. J. Guo and L. Zhao, *Nano Res.* 2024, **17**, 7415−7426.

3. J. Tan, S. Y. Wu, Q. Q. Cai, Y. Wang and P. Zhang, *J. Pharm. Anal.* 2022, **12**, 113−121.

4. B. L. Xu, H. Wang, W. W. Wang, L. Z. Gao, S. S. Li, X. T. Pan, H. Y. Wang, H. L. Yang, X. Q. Meng, Q. W. Wu, L. R. Zheng, S. M. Chen, X. H. Shi, K. L. Fan, X. Y. Yan and H. Y. Liu, *Angew. Chem. Int. Edit.* 2019, **58**, 4911.

5. Y. Wang, G. R. Jia, X. Q. Cui, X. Zhao, Q. H. Zhang, L. Gu, L. R. Zheng, L. H. Li, Q. Wu, D. Singh, D. Matsumura, T. Tsuji, Y. T. Cui, J. X. Zhao and W. T. Zheng, *Chem* 2021, **7**, 436.

6. H. Y. Yan, Y. F. Chen, L. Jiao, W. L. Gu and C. Z. Zhu. *Sensor. Actuat. B-Chem.* 2021, **341**, 130007.